

Wide-Range Probing of Dzyaloshinskii–Moriya Interaction

Duck-Ho Kim,¹ Sang-Cheol Yoo,^{1,2} Dae-Yun Kim,¹ Byoung-Chul Min,² and Sug-Bong Choe^{1†}

¹Department of Physics and Institute of Applied Physics, Seoul National University, Seoul, 08826, Republic of Korea.

²Center for Spintronics, Korea Institute of Science and Technology, Seoul, 02792, Republic of Korea.

†Correspondence to: sugbong@snu.ac.kr

Dzyaloshinskii–Moriya interaction (DMI) in magnetic objects is of enormous interest, because it generates a built-in chirality of magnetic domain walls (DWs) and topologically-protected skyrmions for efficient motion driven by spin–orbit torques. Because of its importance for perspective applications and academic curiosities, many experimental efforts have been devoted to DMI investigation. However, current experimental probing techniques cover only limited ranges of the DMI with specific sample requirements, and there are no versatile techniques covering a wide range of DMI. Here, we present a unique experimental scheme to quantify DMI over a wide range based on the angular dependence of asymmetric DW motion. It can determine DMI even larger than the maximum magnetic field strength, demonstrating that various strengths of DMI can be quantified using a single measurement setup. This scheme provides a standard technique over a wide range of DMI, which is essential to DMI-related emerging fields in nanotechnology.

Introduction

Dzyaloshinskii–Moriya interaction (DMI) is an antisymmetric exchange interaction that occurs at interfaces between ferromagnetic and heavy metal layers with a large spin–orbit coupling^{1–3}. In magnetic systems, DMI generates chiral spin textures such as Néel domain walls (DWs)^{4–7} and magnetic skyrmions^{8–10}. Because these chiral spin textures promise several perspective applications^{4,7,8}, it is crucial to quantify the strength of DMI for physical exploration toward the origin of DMI and technical optimization of DMI strength in ferromagnetic materials.

To measure DMI strength, several experimental schemes have been proposed^{11–15}. Use an optical microscope, Je et al.¹¹ developed a scheme to estimate DMI strength based on asymmetric DW speed with respect to in-plane magnetic field^{11,16,17}. Moon et al.¹² suggested another scheme based on frequency nonreciprocity, which provides a way to measure the DMI constant. Other measurement schemes based on the nonreciprocal propagation of spin waves were also demonstrated using the Brillouin light scattering (BLS)^{18–20} and inductive ferromagnetic resonance (FMR)²¹ techniques. These techniques are applicable to different measurement ranges of DMI strength with different sample requirements.

The optical microscopy technique^{11,16,17} based on asymmetric DW speed provides an easy and simple way to directly measure DMI-induced effective magnetic fields. However, its measurement range is limited by the maximum strength of an external magnetic field, which is limited fundamentally by the narrow available space inside the optical setup. Moreover, application of a large external magnetic field to the optical setup requires sophisticated care to prevent artifacts caused by stray fields from electromagnets as well as mechanical, optical, and thermal artifacts from such strong magnetic fields. In this study, we propose a way to overcome the field strength limit by utilizing angled DWs with respect to the direction of an

in-plane magnetic field.

Results

DW energy model for a DW with an angle θ

The case where a DW is placed with an angle θ with respect to an in-plane magnetic field is shown in the inset of Fig. 1. The DW energy density σ_{DW} can be expressed as a function of the in-plane magnetic field H_x and magnetization angle ψ from the direction normal to the DW:

$$\sigma_{\text{DW}}(H_x, \psi) = \begin{cases} \sigma_0 + 2\lambda K_D \cos^2 \psi \\ -\pi\lambda M_S [(H_x \cos \theta + H_{\text{DMI}}) \cos \psi + H_x \sin \theta \sin \psi] \end{cases} \quad (1)$$

where σ_0 is the Bloch-type DW energy density, λ is the DW width, K_D is the DW anisotropy energy density, M_S is the saturation magnetization, and H_{DMI} is the DMI-induced effective magnetic field in the direction normal to the DW. The second term in the equation corresponds to the DW anisotropy energy and the third term corresponds to the Zeeman energy. Note that Eq. (1) is identical to the Stoner–Wohlfarth equation²² for torque magnetometry with an additional unidirectional bias from H_{DMI} .

For a given H_x , the equilibrium angle ψ_{eq} can be obtained by the minimization condition $\partial\sigma_{\text{DW}}/\partial\psi|_{\psi_{\text{eq}}} = 0$. Moreover, a numerical estimation of Eq. (1) shows that σ_{DW} has a maximum at $H_x = H_0$, where H_0 can be obtained from the maximization condition $\partial\sigma_{\text{DW}}/\partial H_x|_{H_0} = 0$. By solving these minimization and maximization conditions simultaneously, one can readily obtain two coupled equations:

$$4K_D \cos \psi_{\text{eq}} \sin \psi_{\text{eq}} - \pi M_S [(H_0 \cos \theta + H_{\text{DMI}}) \sin \psi_{\text{eq}} - H_0 \sin \theta \cos \psi_{\text{eq}}] = 0, \quad (2)$$

$$\cos \theta \cos \psi_{\text{eq}} + \sin \theta \sin \psi_{\text{eq}} = 0. \quad (3)$$

Equation (3) is identical to the relation $\psi_{\text{eq}} = \theta \mp \pi/2$, which implies the DW magnetization stays perpendicular to the direction of H_0 . Replacing ψ_{eq} using of this relation, Eq. (2) can be rewritten as

$$H_0 = (\pm H_K \sin \theta - H_{\text{DMI}}) \cos \theta, \quad (4)$$

where $H_K (\equiv 4K_D/\pi M_S)$ is the DW anisotropy field. The sign of the first term on the right-hand side of Eq. (4) follows that of H_{DMI} , i.e., a plus sign for a positive H_{DMI} and a minus sign for a negative H_{DMI} . Note that the well-known relation $H_0 = -H_{\text{DMI}}$ ^{11,16,17} can be restored in the limit $\theta \rightarrow 0$. Figure 1 plots $H_0(\theta)$ obtained from Eq. (4) (red solid line) together with the numerical solution (black symbols) from Eq. (1). The exact conformity verifies the validity of Eq. (4).

Equation (4) delivers the key idea of this study: one can largely reduce H_0 by increasing θ . With this scheme, the magnitude of H_0 can be adjusted down to a small experimental range H_{range} of the external magnetic field, which enables one to measure a large H_{DMI} without upgrading the electromagnet. For example, by tilting the DWs up to about 80° , one can measure H_{DMI} up to 1 T using an electromagnet with $H_{\text{range}} \sim 200$ mT, which is quite comfortable for conventional optical setups²³. It is also worth noting that this approach enables one to avoid a number of artifacts from large magnetic fields, such as mechanical instability caused by the induced magnetic moment in the optical setup, magneto-optical effect of the objective lens, and large Joule heating caused by the huge current through the electromagnet.

Verification of θ -dependence in Pt/Co/AlO_x films

To verify the feasibility, the present scheme is applied to ferromagnetic Pt/Co/AlO_x films, of which H_{DMI} is slightly smaller than H_{range} . The measurement procedure of H_0 follows Ref. 11, except for initially tilted DWs. The tilted DWs were generated using the thermomagnetic writing technique^{7,24}. The images on the right-hand side of Fig. 2 show the displacements of the DWs for various θ values with respect to the direction of H_x ($=120$ mT) under the application of a fixed out-of-plane magnetic field H_z ($=5.5$ mT) bias. Each image was obtained by adding several sequential images during the DW displacement with a constant time step ($= 500$ ms), and thus, each image simultaneously shows several DWs moving from brighter to darker interfaces in time. One can then measure the DW speed v for each image. The plots on the left-hand side of Fig. 2 shows the normalized DW speed v/v_{min} in the direction normal to the DW as a function of H_x , where v_{min} is the apparent minimum of v . It can be seen that $v(H_x)$ is symmetric under inversion with respect to H_0^* as shown in each plot. Here, H_0^* indicates the inversion symmetry axis where v has a minimum. According to Ref. 11, v follows the creep relation $\ln[v(H_x)/v_0] \propto -[\sigma_{\text{DW}}(H_x)]^{1/4}$, where v_0 is the characteristic speed. For the case of clear inversion symmetry with a constant v_0 , the experimental H_0^* exactly matches H_0 , and thus, we will denote H_0^* by H_0 hereafter.

Figure 3a plots the measured H_0 with respect to θ . The red solid line shows the best fit by Eq. (4). The good conformity between the data and fitting curve supports again the validity of the equation. The best fitting parameter H_{DMI} ($= -132 \pm 3$ mT) well matches the experimental value ($= -134 \pm 6$ mT) measured at $\theta = 0$. Moreover, the best-fit parameter of H_K ($= -18 \pm 5$ mT) falls within the range of previous experimental reports^{11,25,26}. The value of H_K can be alternatively measured using independent measurements^{11,25,26} or estimated using the relation $H_K \cong (4 \ln 2 / \pi^2) M_S t_f / \lambda^{27,28}$, where t_f is thickness of the magnetic layer.

Application of present scheme to Pt/Co/AlO_x and Pt/Co/MgO films

To mimic the situation that H_{range} is limited (< 50 mT), the fitting is applied only for the data (box in the plot) with large θ ($\geq 70^\circ$) as shown in Fig. 3b. The blue solid line indicates the best fit by Eq. (4) with the fixed value of H_K obtained from Fig. 3a. This approach gives the best-fit parameter H_{DMI} ($= -138 \pm 12$ mT), which matches again previous values within the experimental accuracy. It is therefore demonstrated that the present approach enables one to measure large H_{DMI} in an experiment with limited H_{range} . Note that the determined H_{DMI} is larger than twice of H_{range} .

Because the fitting in Fig. 3b is done with a fixed H_K , here we examine the effect of the inaccuracy δH_K on H_K . The blue dotted lines in Fig. 3b are the best fits for the cases with $\delta H_K = \pm 10$ mT. The error δH_{DMI} is found to be slightly smaller than δH_K , as expected from the relation $\delta H_{\text{DMI}} = \delta H_K \sin \theta$ for θ in Eq. (4). Because H_K is commonly within the range of a few tens of mT^{11,25,26,27,29}, δH_K may not typically exceed the range of about ± 10 mT, and thus one can confirm that δH_K -induced error is not significantly large comparison with other experimental errors. Moreover, this error becomes negligible in practical cases because the present approach is designed for determination of large H_{DMI} ($\gg \delta H_K$) beyond the experimental H_{range} .

Finally, the present scheme is applied to Pt/Co/MgO films, which exhibit DMI larger than H_{range} . Figure 4a shows ν as a function of H_x for $\theta = 0$. This plot clearly shows that the inversion symmetry axis H_0 is beyond the experimental H_{range} (i.e., $H_0 \gg 200$ mT), and thus conventional optical schemes cannot quantify H_{DMI} . However, by applying the present scheme, Fig. 4b shows the measured H_0 with respect to θ for a large range of θ ($\geq 80^\circ$). The black box in the figure indicates the measurable window for H_{range} of the present

setup. The best fit (blue solid line) of H_K ($= -30 \pm 5$ mT) indicates that $H_{\text{DMI}} = -483 \pm 10$ mT, which is more than twice larger than H_{range} . The sign and magnitude are confirmed to match previously reported results²¹. The blue dotted lines in Fig. 4(b) are the best fits for the cases with $\delta H_K = \pm 10$ mT, and thus it is clearly demonstrated that the error becomes negligible in this case.

Discussion

Additional asymmetry from chiral damping³⁰ or asymmetric DW width variation²⁷ may cause a shift δH_0 in H_0 . However, because the asymmetric slope in v caused by these phenomena appears only during chirality variation occurring within the range of $\pm H_K$, $|\delta H_0|$ is essentially smaller than $|H_K|$. Therefore, δH_0 -induced errors are negligible again in practical cases for large H_{DMI} determination.

In conclusion, we proposed a scheme to quantify H_{DMI} over a wide range by overcoming the limitation from H_{range} . By measuring the angular dependence of asymmetric DW motion, we clearly find that the H_0 has the clearly angle dependence, in a robust manner quantifying the large DMI with large θ . The feasibility of the present scheme is demonstrated experimentally for various strengths of DMI using ferromagnetic Pt/Co/AlO_x and Pt/Co/MgO films. The errors caused by additional asymmetry and inaccuracy of H_K were found to be negligible in practical cases for large H_{DMI} determination. The present scheme enhances the experimental range of optical measurement techniques without upgrading electromagnets. Our finding opens a novel way to easy and straightforward manner to explore materials and systems for large DMI, and thus surmounts the key obstacle to design emerging devices with tailoring the DMI for topological stability and efficient manipulation as required for next-generation nanotechnology.

References

1. Dzialoshinskii, I. E. Thermodynamic theory of weak ferromagnetism in antiferromagnetic substances. *Sov. Phys. JETP* **5**, 1259-12172 (1957).
2. Moriya, T. Anisotropic superexchange interaction and weak ferromagnetism. *Phys. Rev.* **120**, 91-98 (1960).
3. Thiaville, A., Rohart, S., Jué, É., Cros, V. & Fert, A. Dynamics of Dzyaloshinskii domain walls in ultrathin magnetic films. *Europhys. Lett.* **100**, 57002 (2012).
4. Parkin, S. & Yang, S.-H. Memory on the racetrack. *Nature Nanotech.* **10**, 195-198 (2015).
5. Ryu, K.-S., Thomas, L., Yang, S.-H. & Parkin, S. Chiral spin torque at magnetic domain walls. *Nature Nanotech.* **8**, 527-533 (2013).
6. Yang, S.-H., Ryu, K.-S. & Parkin, S. Domain-wall velocities of up to 750 m s^{-1} driven by exchange-coupling torque in synthetic antiferromagnets. *Nature Nanotech.* **10**, 221-226 (2015).
7. Moon, K.-W. *et al.* Magnetic bubblecade memory based on chiral domain walls. *Sci. Rep.* **5**, 9166 (2015).
8. Fert, A., Cros, V. & Sampaio, J. Skyrmions on the track. *Nature Nanotech.* **8**, 152-156 (2013).
9. Sampaio, J., Cros V., Rohart, S., Thiaville, A., & Fert, A. Nucleation, stability and current-induced motion of isolated magnetic skyrmions in nanostructures. *Nature Nanotech.* **8**, 839-844 (2013).
10. Jiang, W. *et al.* Blowing magnetic skyrmion bubbles. *Science* **349**, 283-286 (2015).

11. Je, S.-G. *et al.* Asymmetric magnetic domain-wall motion by the Dzyaloshinskii-Moriya interaction. *Phys. Rev. B* **88**, 214401 (2013).
12. Moon, J.-H. *et al.* Spin-wave propagation in the presence of interfacial Dzyaloshinskii-Moriya interaction. *Phys. Rev. B* **88**, 184404 (2013).
13. Pizzini, S. *et al.* Chirality-induced asymmetric magnetic nucleation in Pt/Co/AlO_x ultrathin microstructures. *Phys. Rev. Lett.* **113**, 047203 (2014).
14. Han, D.-S. *et al.* Asymmetric hysteresis for probing Dzyaloshinskii-Moriya interaction. *Nano Lett.* DOI:10.1021/acs.nanolett.6b01593 (2016).
15. Dmitrienko, V. E. *et al.* Measuring the Dzyaloshinskii–Moriya interaction in a weak ferromagnet. *Nature Phys.* **10**, 202-206 (2014).
16. Hrabec, A. *et al.* Measuring and tailoring the Dzyaloshinskii-Moriya interaction in perpendicularly magnetized thin films. *Phys. Rev. B* **90**, 020402(R) (2014).
17. Kim, D.-H., Yoo, S.-C., Kim, D.-Y., Min, B.-C. & Choe, S.-B. Universality of Dzyaloshinskii-Moriya interaction effect over domain-wall creep and flow regimes. arXiv:1608.01762 (2016).
18. Belmeguenai, M. *et al.* Interfacial Dzyaloshinskii-Moriya interaction in perpendicularly magnetized Pt/Co/AlO_x ultrathin films measured by Brillouin light spectroscopy. *Phys. Rev. B* **91**, 180405(R) (2015).
19. Cho, J. *et al.* Thickness dependence of the interfacial Dzyaloshinskii–Moriya interaction in inversion symmetry broken systems. *Nat. Commun.* **6**, 7635 (2015).

20. Nembach, H. T., Shaw, J. M., Weiler, M., Jué, E. & Silva, T. J. Linear relation between Heisenberg exchange and interfacial Dzyaloshinskii–Moriya interaction in metal films. *Nature Phys.* **11**, 825-829 (2015).
21. Lee, J.-M., Jang, C., Min, B.-C., Lee, K.-J. & Chang, J. All-electrical measurement of interfacial Dzyaloshinskii-Moriya interaction using collective spin-wave dynamics. *Nano Lett.* **16**, 62–67 (2016).
22. Stoner, E. C. & Wohlfarth, E. P. A Mechanism of magnetic hysteresis in heterogeneous alloys. *Philosophical Transactions of the Royal Society A: Physical, Mathematical and Engineering Sciences* **240**, 599–642 (1958).
23. Kim, D.-H. *et al.* Maximizing domain-wall speed via magnetic anisotropy adjustment in Pt/Co/Pt films. *Appl. Phys. Lett.* **104**, 142410 (2014).
24. Moon, K.-W. *et al.* Distinct universality classes of domain wall roughness in two-dimensional Pt/Co/Pt films. *Phys. Rev. Lett.* **110**, 107203 (2013).
25. Haazen, P. P. J., Murè, E., Franken, J. H., Lavrijsen, R., Swagten, H. J. M. & Koopmans, B. Domain wall depinning governed by the spin Hall effect. *Nature Mater.* **12**, 299-303 (2013).
26. Emori, S. *et al.* Spin Hall torque magnetometry of Dzyaloshinskii domain walls. *Phys. Rev. B* **90**, 184427 (2014).
27. Kim, D.-Y., Kim, D.-H. & Choe, S.-B. Intrinsic asymmetry in chiral domain walls due to the Dzyaloshinskii–Moriya interaction. *Appl. Phys. Express* **9**, 053001 (2016).

28. Jung, S.-W., Kim, W., Lee, T.-D., Lee, K.-J. & Lee, H.-W. Current-induced domain wall motion in a nanowire with perpendicular magnetic anisotropy. *Appl. Phys. Lett.* **92**, 202508 (2008).
29. Je, S.-G., Yoo, S.-C., Kim, J.-S., Moon, J., Min, B.-C. & Choe S.-B. Drastic emergence of huge negative spin-transfer torque in atomically thin Co layers. arXiv:1512.03405v1 (2015).
30. Jué, E. *et al.* Chiral damping of magnetic domain walls. *Nature Mater.* **15**, 272-277 (2016).

Figure Captions

Figure 1. **Plot of H_0 as a function of θ .** Black symbols are obtained by the numerical solution from Eq. (1) and red solid line is calculated by Eq. (4). The inset is schematic illustration for measurement.

Figure 2. **Plot of v/v_{\min} with respect to H_x fixed H_z and under various θ in Pt/Co/AlO_x film.** **a**, 0° **b**, 30° **c**, 60°, and **d**, 90°. Displacement driven by a magnetic field for DWs at each angle.

Figure 3. **Plot of the measured H_0 with respect to θ in Pt/Co/AlO_x film.** **a**, Collected data with large θ ranges from 0° to 90°. The red solid line shows the best fit by Eq. (4). **b**, Collected data with small θ ranges from 70° to 90°. The blue solid line exhibits the best fit by Eq. (4) with the fixed value of H_K . The blue dotted lines in Fig. 3(b) are the best fits for the cases with $\delta H_K = \pm 10$ mT, respectively.

Figure 4. **DMI determination in Pt/Co/MgO film.** **a**, Plot of the measured v with respect to H_x fixed $H_z = 20$ mT at $\theta = 0$. **b**, Plot of the measured H_0 with respect to θ for the θ ranges from 80 to 90°. The blue solid line exhibits the best fit by Eq. (4) and the blue dotted lines in Fig. 4(b) are the best fits for the cases with $\delta H_K = \pm 10$ mT, respectively.

Methods

Methods and any associated references are available in the online version of the paper.

Acknowledgements

This work was supported by a National Research Foundations of Korea (NRF) grant that was funded by the Ministry of Science, ICT and Future Planning of Korea (MSIP) (2015R1A2A1A05001698 and 2015M3D1A1070465). D.-H.K. was supported by a grant funded by the Korean Magnetics Society. B.-C.M. was supported by the KIST institutional program and Pioneer Research Center Program of MSIP/NRF (2011-0027905).

Author contributions

D.-H.K. planned and designed the experiment and S.-B.C. supervised the study. D.-H.K. and D.-Y.K. carried out the measurement. S.-C.Y. and B.-C.M. prepared the samples. S.-B.C. and D.-H.K. performed the analysis and wrote the manuscript. All authors discussed the results and commented on the manuscript.

Additional information

Correspondence and request for materials should be addressed to S.-B.C.

Competing financial interests

The authors declare no competing financial interests.

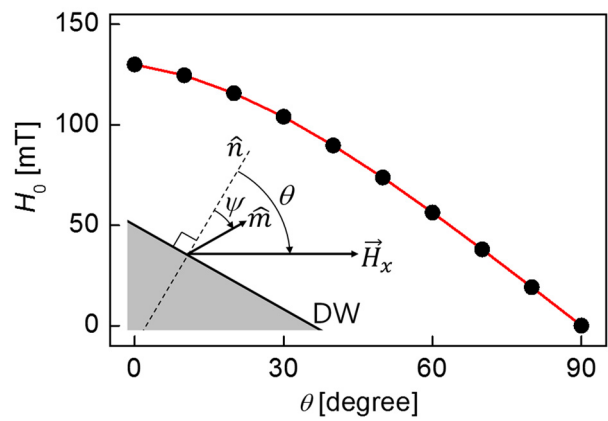


Figure 1

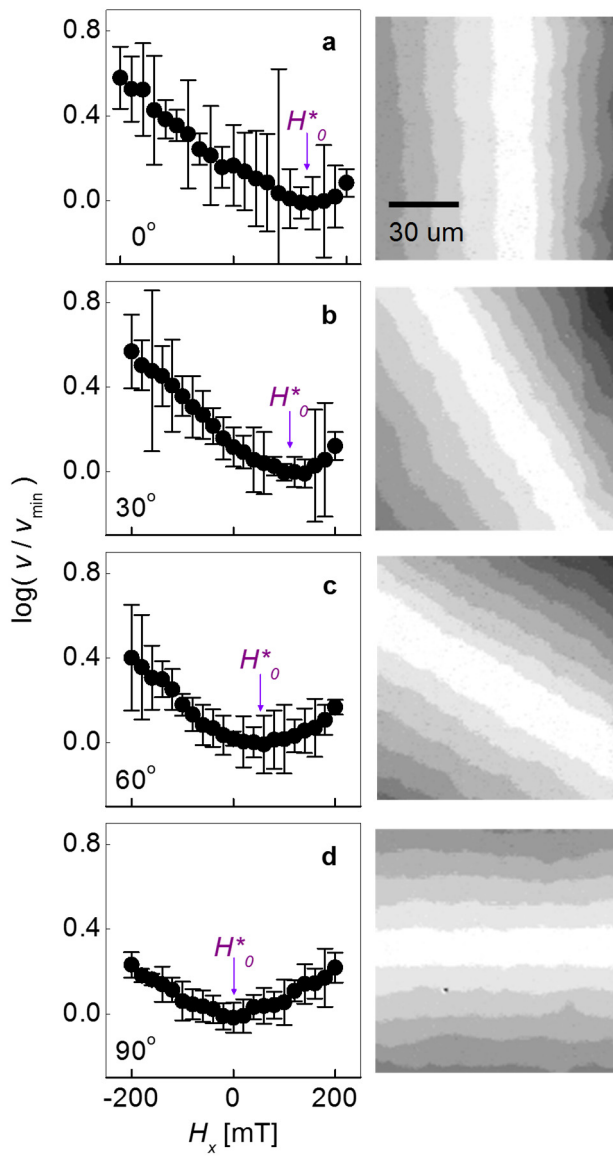


Figure 2

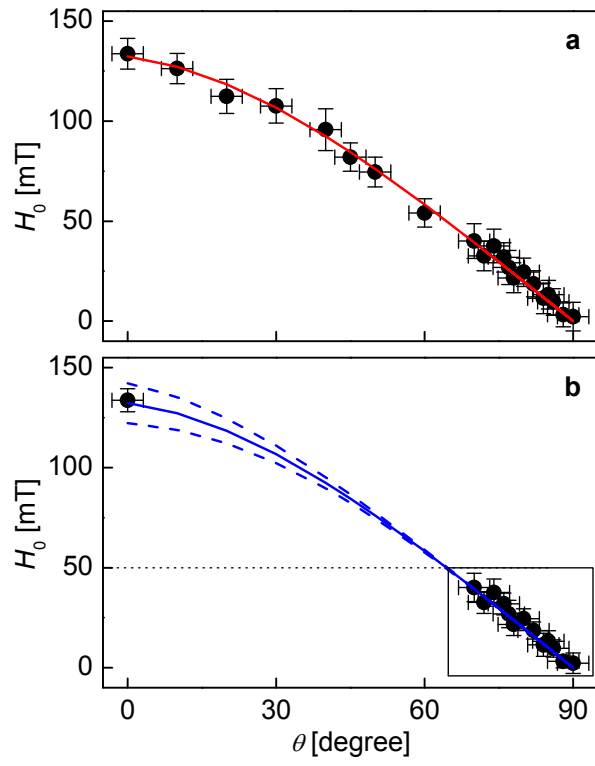


Figure 3

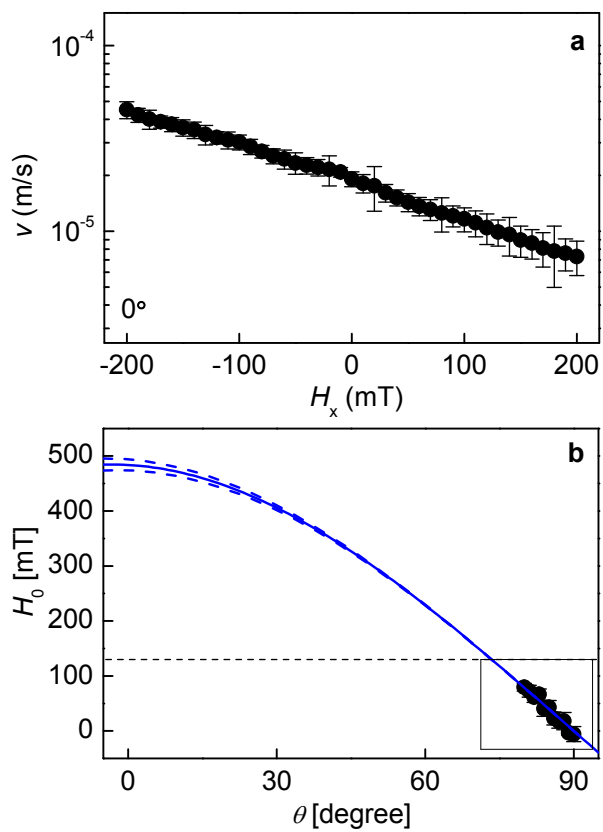


Figure 4